CLM-P92

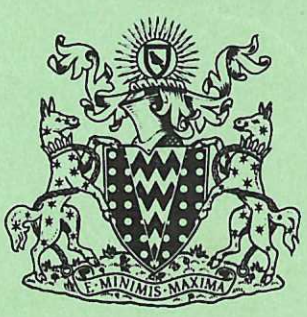

United Kingdom Atomic Energy Authority

RESEARCH GROUP

Preprint

EXPERIMENTAL OBSERVATIONS OF COLLISIONLESS SHOCK WAVES IN A MAGNETIZED PLASMA

J. W. M. PAUL
M. J. PARKINSON
J. SHEFFIELD
L. S. HOLMES

Culham Laboratory,

Culham, Abingdon, Berkshire

1965

UNCLASSIFIED
(Approved for Publication)

CLM - P 92

EXPERIMENTAL OBSERVATIONS OF COLLISIONLESS SHOCK WAVES IN A MAGNETIZED PLASMA

By

J.W.M. Paul
M.J. Parkinson
J. Sheffield
L.S. Holmes

A B S T R A C T

Electric and magnetic field measurements within the structure of a shock front are presented. The shock front propagates through a highly ionized plasma in a direction perpendicular to a magnetic field. The dynamics of the driving piston, a linear Z-pinch, and of the shock wave are shown to agree with theory. At low Alfven Mach number ($M_A < 3$) the structure measurements are consistent with a shock mechanism based on electron drift instabilities. This 'resistive' mechanism is theoretically inadequate for $M_A > 3$. The experimentally observed change of structure for $M_A \geq 3$ is interpreted as evidence for an additional, but as yet unidentified collisionless mechanism.

U.K.A.E.A. Research Group,
Culham Laboratory,
Abingdon,
Berks.

November, 1965

CONTENTS

1. INTRODUCTION

This paper describes a study in progress at Culham Laboratory on strong shock waves in a magnetized plasma /1,2,3,4/. The aim is to study the structure of collision free shock fronts and determine the mechanisms of energy dissipation.

Measurements of the structure of shock fronts, propagating through a plasma in a direction perpendicular to a magnetic field, are presented. Most of the information has been obtained by using magnetic and electric probes in the plasma. At low Alfven Mach number [ratio of shock velocity (V_s) to initial Alfven velocity] $M_A < 3$ the results are consistent with a mechanism based on collisionless turbulence derived from electron drift instabilities. At higher M_A (> 3) theory predicts that this mechanism by itself is not adequate. Experimental evidence is presented for the existence of an additional but as yet unidentified collisionless mechanism in shocks with $M_A > 3$.

The shock wave is produced by a fast linear Z-pinch between electrodes with 100 cm separation in a fused silica tube of 50 cm diameter. The applied axial electric field (E_z) produces an axial current which rises to several 100 kA in a fraction of a microsecond and flows in a thin annular layer (~ 1 cm). The resulting pinch forces drive this skin current radially inwards at a velocity (10 - 15 cm/μsec) exceeding the initial Alfven velocity. This rapid radial compression generates an imploding shock wave which propagates ahead of the driving skin current with a velocity between 20 and 50 cm/μsec.

2. TARANTULA EXPERIMENTS (Ref. 5)

After filling the tube with gas to a given pressure ($P_0 \sim 5$ to 20 mT) and establishing a uniform axial magnetic field ($B_{z0} \sim 0.25$ to 1.5 kG), electrical breakdown of the gas is initiated and an axial current (~ 80 kA) heats the gas to a high degree of ionization (~ 90%). The fast pinch is produced by discharging a low inductance (14 nH) capacitor bank (20 μF) through 40 spark gap switches into the initial plasma. For the capacitors charged to V_0 = 75 kV (max. of 100 kV) the measured E_z = 0.62 kV/cm, $(dI/dt)_0 = 1.8 \times 10^{12}$ A/s, and the current rises to 420 kA in 0.5 μsec. For V_0 = 50 kV the corresponding values are E_z = 0.32 kV/cm, $(dI/dt)_0 = 1.1 \times 10^{12}$ A/s, and 310 kA in 0.6 μsec. This bank is inductively coupled to the discharge so that the plasma remains at earth potential. This allows the insertion into the plasma of 'earthy' probes of very small dimensions.

3. THE INITIAL PLASMA

3.1 Formation

The initial plasma through which the shock wave propagates is produced by an oscillatory axial current of about 80 kA peak. Detailed measurements have

been made on the plasma using double electric (Langmuir) and magnetic probes, an infra-red interferometer and an image converter camera. During the first half cycle (~ 50 μsec) the ionization (and current) is confined to the outer half of the tube. This skin behaviour appears to be determined by the slow rate of propagation of ionization into the tube. However after current reversal the plasma becomes turbulent and rapidly diffuses to the centre. The current is clamped on its third peak (~ 170 μsec) and a reproducible quiescent plasma develops. The shock bank is discharged into this plasma when the current is almost zero (310 μsec).

3.2 Electron Density and Temperature

At the time for discharging the shock bank, the axial distribution of electron density (n_e) as measured by a double electric probe is reasonably uniform to within about 1 cm of the electrodes. There it starts falling. The radial distribution of n_e was obtained from a double electric probe and an infra-red interferometer with an axial path. (e.g. Fig.1 for P_0 = 20 mT H_2 B_{zo} = 1.15 kG). The double electric probe indicates an electron temperature of about 1 eV throughout the bulk of the plasma.

3.3 Neutral Particle Density

The total density of particles (ions and neutrals) has been measured for P_0 = 20 mT hydrogen, B_{zo} = 1.15 kG. The total density was obtained from the measured velocity of propagation, in a radial direction, of a small amplitude magnetosonic wave, of low frequency (f). Below a certain critical frequency (f_c) the neutral particles (as well as the ions) are coupled into the wave through charge exchange collisions (cross section $\sigma_{cx} \sim 6 \times 10^{-15}$ cm^2). On a simple theory, if the collision time for a neutral to be hit by an ion ($\tau_{cx} = 1/(n_i \overline{\sigma_{cx} V_i})$) is short compared with the duration of the ion wave motion (~ 1/(2f)), then the neutral moves with the ions. This defines the critical frequency

$$f_c = C\, n_i \overline{\sigma_{cx} V_i}$$

where a value $C = \frac{1}{2}$ is obtained from the simple theory but $C = 1/(2\pi)$ from more exact calculation. For the conditions of the experiment almost complete coupling and uncoupling of the neutrals should occur within ± 30% of f_c. Assuming that the relevant ion velocity is the thermal velocity for a plasma at 1 eV the critical frequency f_c = 940 kc/s.

Experimentally the wave is excited in the initial plasma by a small axial skin current with a basic frequency half the required wave frequency. The radial propagation of the wave, with amplitude about 1% of B_{zo} was observed

on a multiple magnetic probe. The results for two wave frequencies are shown in Fig.2 as space-time streaks. The velocities are independent of radius within experimental errors and correspond to total densities (n_T) with 90% confidence limits as below

340 kc/s wave $n_T = (6.5 \pm 0.5) \times 10^{14}$ cm^{-3}

120 kc/s wave $n_T = (8.5 \pm 1.7) \times 10^{14}$ cm^{-3}

Weighted mean $n_T = (7.0 \pm 0.8) \times 10^{14}$ cm^{-3}

Attempts to propagate the wave slightly above f_c have shown heavy damping of the wave but propagation of sub-harmonics.

The above theories are for infinite plane geometry with uniform densities. The experimental wave is cylindrically converging with a radius smaller than the wave length and with appreciable change of n_e over a wavelength. The validity of the method has been checked by using the 3 fluid (electrons, ions, neutral atoms) version of the M.H.D. plasma collapse computation /6/. Using the measured radial variation of n_e and the measured uniform n_T, a theoretical space-time diagram of the wave propagation is obtained which is in good agreement with experiment (Fig.2). This adds confidence to the result plotted in Fig.1 and reported previously /3/.

3.4 Discussion of Initial Plasma

The above results are interpreted as indicating that the quiescent preheated plasma is confined radially by the axial magnetic field and axially by a layer of neutral gas near the electrodes. The measured peak n_e and uniform n_T corresponds to only half the filling density. The rest of the particles are presumed to have been lost mainly to the ends forming the neutral layer.

The important parameters for the shock structure study are the electron density and the degree of ionization. Both vary appreciably with radius in the outer region but for radius less than 10 cm they are roughly constant with about 90% ionization. Even taking the higher limit of n_T and a 10% reduction on n_e the degree of ionization is 80% on axis and 73% at 10 cm radius.

The electron density measurements have been repeated for different B_{zo}, P_o and for deuterium gas. For P_o = 10 mT, n_e is about half that for 20 mT. Changing to deuterium has little effect on the electron density. For B_{zo}, down to 0.5 kG the flat central electron density is almost independent of B_{zo} but below this it falls with B_{zo}.

4. DYNAMICS OF PLASMA COLLAPSE

4.1 Magnetic Field Measurements

With the initial conditions well documented the next step is to study the pinch and shock dynamics and compare these with theory. The axial and azimuthal magnetic field have been measured during the collapse by using a multiple magnetic probe of 7 mm diameter. Good shot to shot and month to month reproducibility is obtained. The shock front, a sharp jump in axial magnetic field strength, is observed clearly separated from the thin skin current as shown in Figs.3 and 4.

4.2 The Three Phases of Implosion

The shock velocity as a function of radius has been measured accurately by using a small double magnetic probe (3.5 mm diameter) with a frequency response up to about 200 Mc/s (Fig.5). There are three phases of implosion; (i) for $R > 12$ cm the shock is accelerating and steepening; (ii) for 12 cm $> R > 3$ cm the shock velocity and width appear constant forming the steady phase; (iii) for $R < 3$ cm severe convergence produces an increase of velocity. The structure measurements reported are all for $R \sim 9$ cm in the steady phase.

4.3 Comparison with Computation

The dynamics, as measured by magnetic probes, have been compared with the predictions of numerical computation in which the plasma is treated in the two fluid (electrons and ions) M.H.D. approximation /7/. The initial conditions of circuits and plasma are used in the computation. The shock structure predicted by the computation broadens rapidly as viscous effects increase. If viscosity is omitted the structure steepens as the electron temperature increases and resistivity decreases. These shock structure effects, which disagree with the experimental results, have been removed by introducing into the computation an artificially fixed shock width /8/. Good agreement is then obtained between experiment and computation on the dynamics (Figs.3,4) as reported previously /3/, provided the measured initial total density is used rather than the electron density.

5. EXPERIMENTAL METHODS FOR STUDYING SHOCK STRUCTURE

The structure of the magnetic field within the shock front was measured using magnetic probes, sheathed in glass or quartz. The probes were inserted radially across the centre line so that the shock front collapses onto the probe tip. The plasma can part round the probe by moving along the magnetic field lines allowing these lines to pass into the probe. The hole left in

the conducting plasma limits the space resolution to about twice probe diameter /9,10/. A typical oscillogram of dB_z/dt from the 0.9 mm probe is shown in Fig.6.

The structure of the radial potential (V_R) within the shock front was measured using coaxial double electric probes. Again the shock front collapsed onto the probe tip. These probes should respond very rapidly ($\sim 1/\omega_{pi}$) with a resolution limited by the radial extent of the tip ($\sim$ 0.25 mm) or the rise time of the circuit (3 nsec). On one probe the tip separation could be varied from 0.5 mm to 2 cm. This permitted easy discrimination between measurements of total voltage across the shock and the electric field within it. Despite the high electric fields recorded ($\sim$ 4 kV/cm), there was no evidence of electrical breakdown across the probe insulation in contact with the plasma. The short duration of the electric field ($\sim$ 10 nsec) may explain this. The fact that the measured shock width varies with plasma parameters (gas, P_o, B_{zo}) is evidence that the probe dimensions are not a limiting factor. A typical oscillogram for 1 cm tip separation is shown in Fig.6.

6. SHOCK STRUCTURES FOR LOW M_A (< 3)

6.1 Measurements of V_R and B_z in the Shock Front

With the shock bank charged to 50 kV, initial pressure P_o = 20 mT of hydrogen and B_{oz} = 1.15 kG the steady shock velocity of 24 cm/μsec corresponds to M_A = 2.5. The corresponding dynamics was shown in Fig.4. The measured change of magnetic field ($B_z - B_{zo}$) and radial potential V_R within the shock front for radius 9 cm are plotted in Figs.7a and 8. The magnetic probe records a coincident but slightly slower rise than the electric probe as explained in section 5. The measured shock velocity does not vary appreciably with radius so Fig.7 also represents the spatial variations.

6.2 Discussion of Collisional Processes

The measured shock width ($\sim$ 1.4 mm) is appreciably shorter than the appropriate ion-ion and ion-neutral collision lengths (L_{ii}, L_{in}) as shown in Fig.9. Consequently collisional viscosity can be neglected in these experiments as reported previously /3/ and in agreement with the failure of the viscous computation.

The collisional lengths were calculated for the undisturbed ion or neutral charge exchanged to a slow ion, being hit by the ions of the compressed plasma behind the shock. The velocities are taken from the computed dynamics which have been confirmed experimentally.

Resistive dissipation through the azimuthal current in the shock front, is the only other collisional process (electron-ion collisions) capable of sustaining such a shock /11/. Unfortunately it cannot be eliminated by such a simple criterion. The above measured rise time of V_R (6 nsec) is less than two electron-ion thermal collision times (Fig.9). The latter is calculated for the region behind the shock assuming that the shock heating, required by the dynamics, goes entirely to the electrons ($T_e \sim 50$ eV). By changing to deuterium at half the pressure the dynamics remain the same but the electron temperature should be 100 eV. The measured rise time of 13 nsec then corresponds to only half the predicted electron-ion collision time.

6.3 Discussion of Electron Temperature

The calculated electron-ion collision times depend on assuming that the predicted electron temperature (T_e) is in fact achieved. Although no direct measurement of T_e has as yet been made, indirect evidence (section 6.4) confirms the predicted value. If the electrons are heated to the predicted 50 eV in the shock front, as appears probable, calculation shows that the rate of loss of energy by radiation and conduction to the ends is negligible during the 6 nsec heating time of the shock front.

The measured neutron output of about 10^5 per shot for $V_o = 75$ kV, $P_o = 10$ mT deuterium, $B_{zo} = 1.15$ kG occurs after the shock wave converges on the axis. Thereafter neutrons are emitted for about a microsecond. Unfortunately this cannot be used as evidence against ion heating during the implosion. But it is evidence for a rapid collisionless spreading of the directed ion velocities on convergence.

6.4 Radial Voltage Across the Shock Front

The change in directed energy of an ion passing through the shock front (considered at rest) is $\Delta W = \frac{1}{2} M [V_s^2 - (V_s - V_p)^2]$ where M is the ion mass and V_p is the plasma velocity behind the shock (laboratory coordinates). The latter has been derived from the measured magnetic field profiles using the fact that (B_z/n_e) is constant across shock (though not within it). The measured azimuthal electric field E_θ behind the shock also provides a measure of V_p $(= E_\theta/B_z)$. The measured radial voltage across the shock is such that the ratio $Q = eV_R/\Delta W = 1.03 \simeq 1.0$. This means that the ion motion through the shock is entirely accounted for by electric field effects.

The following conclusions can be derived from the equations of motion of the electrons and ions through the shock front. If the diamagnetic ion current is allowed to flow

$$Q = \frac{eV_R}{\Delta W} = 1 \quad \text{and} \quad ne\, E_R = J_\theta \times B_z - \nabla (p_i + p_e)$$

where E_R is radial electric field, J_θ azimuthal current density in the shock and ∇p is pressure gradient. However if conservation of angular momentum prevents the diamagnetic ion current

$$Q = 1 - \frac{1}{\Delta W}\int_1^2 \frac{\nabla p_i}{n_e}\, dr \quad \text{and} \quad ne\, E_R = J_\theta \times B_z - \nabla p_e \ .$$

In this case $Q = 1$ implies $\nabla p_i = 0$ and E_R depends on ∇p_e.

It is unlikely that azimuthal angular momentum can be introduced into the shock on the required time scale. This requires some further study. Consequently it seems probable that the measured $Q = 1$ implies negligible ion heating and appreciable electron heating. The measured radial variation of V_R (for P_o = 20 mT, H_2, B_{zo} = 1.15 kG, V_o = 50 kV) is compared (Fig.10) with that to be expected on the above theory using computed parameters assuming electron heating (curve A) and alternatively assuming ion heating without ion current (curve B). Over the range of radii from 5 to 12 cm there is good agreement with the predicted electron heating.

6.5 Collisionless Interpretation

It seems unlikely that collisional resistivity can account for the observed shock structure. A possible collisionless mechanism is provided by electron-ion drift instabilities /12,13/. The measurements for $M_A = 2.5$ in hydrogen indicate an electron drift velocity (V_D) which is about 10% of the predicted electron thermal velocity (V_{th}). Note that if the temperature was lower than predicted, (V_D/V_{th}) would be proportionately larger. With (V_D/V_{th}) $\geq$ 0.1, Stringer /14/ predicts that drift instabilities should occur provided $T_i \leq 0.1\ T_e \sim 5$ eV. This required ion temperature corresponds with that to be expected from the reversible heating of the initial plasma.

The measured shock width for $M_A = 2.5$ in hydrogen corresponds to $7(c/\omega_{pe})$ for the initial conditions while that for $M_A = 2.5$ in deuterium is 10 (c/ω_{pe}). It is easily shown that if drift instabilities limit the drift velocity to some critical ratio $(V_D/V_{th})^*$ the shock width

$$L \sim \left(\frac{V_{th}}{V_D}\right)^* \left(\frac{c}{\omega_{pe}}\right)$$

The above measurements indicate a smaller critical ratio $(V_D/V_{th})^*$ in deuterium. As the ratio T_i/T_e is halved for the deuterium experiment Stringer would predict a smaller ratio.

7. CRITICAL ALFVEN MACH NUMBER

With resistivity (whether collisional or not) as the only dissipative

mechanism, continuum theory fails for M_A greater than a critical value $M_A^* \sim 3$, /11/. Physically beyond this limit slip of the field and plasma (resistive dissipation) cannot by itself provide sufficient dissipation of energy. Theories based on particle orbits predict the occurrence of multiple streaming of the ions above a similar limit /15/. The shock is said to have 'broken' and again a solution for the structure cannot be obtained without introducing a non-resistive process.

Experimentally M_A has been increased by reducing the initial axial magnetic field. For these strong shocks this does not appreciably affect the shock velocity. For different initial conditions (H_2, D_2, P_o = 10 and 20 mT, V_o = 35 and 50 kV) the shock structure undergoes an appreciable change (described in the next section) within the range $2.5 < M_A < 3.1$. This is in good agreement with the theoretical predictions.

8. SHOCK STRUCTURE AT HIGH M_A (> 3)

Above the critical $M_A(\sim 3)$, the shock has a clear double structure on V_R and B_Z. The sharp transition ($\sim$ 1.4 mm) is preceeded by a broad feature ($\sim$ 1.5 cm) corresponding to $(2c/\omega_{pi})$ in the initial plasma. A typical structure for $M_A = 3.7$ in hydrogen is shown in Fig.7b (R = 9 cm). The measured radial voltage across the shock corresponds to $Q = 0.9 \simeq 1.0$ suggesting that the electrons are heated.

At still higher M_A the broad structures forward and to the rear of the sharp transition become dominant and at $M_A \sim 6$ (Fig.8) the sharp transition is absent. The total structure is then so broad that cylindrical effects are important.

The broad additional feature at $M_A = 3.7$ is shorter than the ion-ion mean free path but is comparable with the ion-neutral mean free path used in section 6.2. Even so this latter mechanism can be neglected because at least five such collisions are required to collect the undisturbed ions (> 80% ionized). Electron-thermal conductivity, another relevant collisional mechanism /16/ is made negligible by the presence of the axial magnetic field /17/. Consequently all collisional mechanisms appear to be eliminated for $M_A > M_A^*$.

9. COLLISIONLESS SHOCK THEORIES FOR $M_A > 3$

Of the many theories of collisionless shocks only a few are valid for $M_A > M_A^*$. Theories involving ion-ion streaming instabilities /18,19/ or Landau damping of electron oscillation /20/ can be eliminated because they predict a much sharper transition. Auer et al /21/ treat the problem of ion streaming

without instabilities but derive an effective entropy increase from ion gyration phase mixing and assume that the electrons are not heated. This approach leads to a broad time dependent structure with $Q = 0.25$ (for $M_A = 6$). Carmac et al /22/ describe a model based on non-linear wave-wave interaction within a front of width $L \sim \frac{2c}{\omega_{pi}}$ for $M_A \sim 4$ but steepening with increasing M_A. The particular analysis, though not the mechanism, is limited to low M_A ($< M_A^*$). Although no explicit prediction is made, it is reasonable to assume that the waves involved ($\omega \gg \omega_{ci}$) heat the electrons and consequently $Q = 1$. These values of L and Q are comparable with those of the broad feature but the dependence on M_A appears inconsistent.

Experimental imperfections make it possible that the magnetic field makes a small angle $\left(\theta > \sqrt{\frac{M_e}{M_p}} \sim 1^o\right)$ to the shock front. This leads theoretically /23,24/ to a structure more than an order of magnitude too short and consequently it has been neglected.

10. CONCLUSION

In summary, at low Mach numbers ($M_A < 3$) the results indicate that a resistive shock is formed which probably involves collisionless turbulence. Above the predicted critical $M_A(\sim 3)$ the observed change of structure is interpreted as due to an additional, but unidentified, collisionless mechanism. None of the present theories of shock structure gives convincing agreement over the range of observations but some can be eliminated.

ACKNOWLEDGEMENTS

The authors wish to acknowledge the encouragement and guidance received from Dr. R.J. Bickerton and the experimental assistance of Mr. C.A. Steed.

REFERENCES

1. ASHBY, D.E.F.T. and PAUL, J.W.M. 4th Int. Conf. on Ionization Phenomena in Gases. (1959) 961.

2. ASHBY, D.E.T.F., ROBERTS, K.V. and ROBERTS, S.J. N. Nucl. Energy Pt C, 3, (1961) 162.

3. PAUL, J.W.M., HOLMES, L.S., PARKINSON, M.J. and SHEFFIELD, J. Bull. Amer. Phys. Soc., series 2, 10, (1965) 223. (Abstract only).

4. PAUL, J.W.M., HOLMES, L.S., PARKINSON, M.J. and SHEFFIELD, J. Nature, 208, (1965) 133. (In the press)

5. BELL, W.R., BISHOP, A.E., CRAWLEY, H.J., EDMONDS, G.D., PAUL, J.W.M. and SHEFFIELD, J. Inst. Elect. Eng. (London) (Submitted for Publication) Culham report no. CLM-P 78.

6. FISHER, D.L., HAIN, K., ROBERTS, K.V. and TAYLOR, I. (Private Communication).

7. HAIN, K., HAIN, G., ROBERTS, K.V., ROBERTS, S.J. and KOPPENDORFER, W. Zelts. fur Nat. 15, (1960), 1039.

8. RICHTMEYER, R.D. Difference Methods for Initial Value Problems, Interscience N.Y. p.208, (1957).

9. DIPPEL, K.H. and TECKENBURG, W. 4th Int. Conf. on Ionization Phenomena in Gases, 1, (1959) 533.

10. MALMBERG, J.H. Rev. Sci. Inst. 35, (1964), 1622.

11. GOLDEN, K.I., SEN, H.K. and TREVE, Y.M. 5th Conf. on Ionization Phenomena in Gases, 2, (1961) 2109.

12. ZAVOISKI, E.K. J. Nucl. Energy Pt.C, 5 (1963) 381.

13. ADLAM, J.H. and HOLMES, L.S. Nucl. Fusion, 3, (1963) 62.

14. STRINGER, T.E. J. Nucl. Energy Pt C, 6, (1964), 267.

15. MORAWITZ, C.S. Phys. Fluids, 4, (1961) 988.

16. MARSHALL, W. Proc. Roy. Soc., (London) A. 233 (1956) 367.

17. CHAPMAN, S. and COWLING, T.G. Mathematical Theory of Non-uniform Gases, Cambridge University Press. (1939).

18. KAHN, F.D. J. Fluid Mech. 2, (1957) 601.

19. PARKER, E.N. Astrophys. J. 129, (1959) 217.

20. COLGATE, S.A. Phys. Fluids, 2, (1959) 485.

21. AUER, P.L., HURWITZ, H. and KILB, R.W. Phys. Fluids, 5 (1962) 298.

22. CARMAC, M., KANTROWITZ, A.R., LIYVAK, M.M., PATRICK, R.M. and PETSCHEK, H.E. Nuclear Fusion supplement Pt.2 (1962) 423.

23. KARPMAN, V.I. Sov. Phys. Tech. Phys. 8 (1964) 715.

24. MORTON, K.W. Phys. Fluids, 7, (1964) 1800.

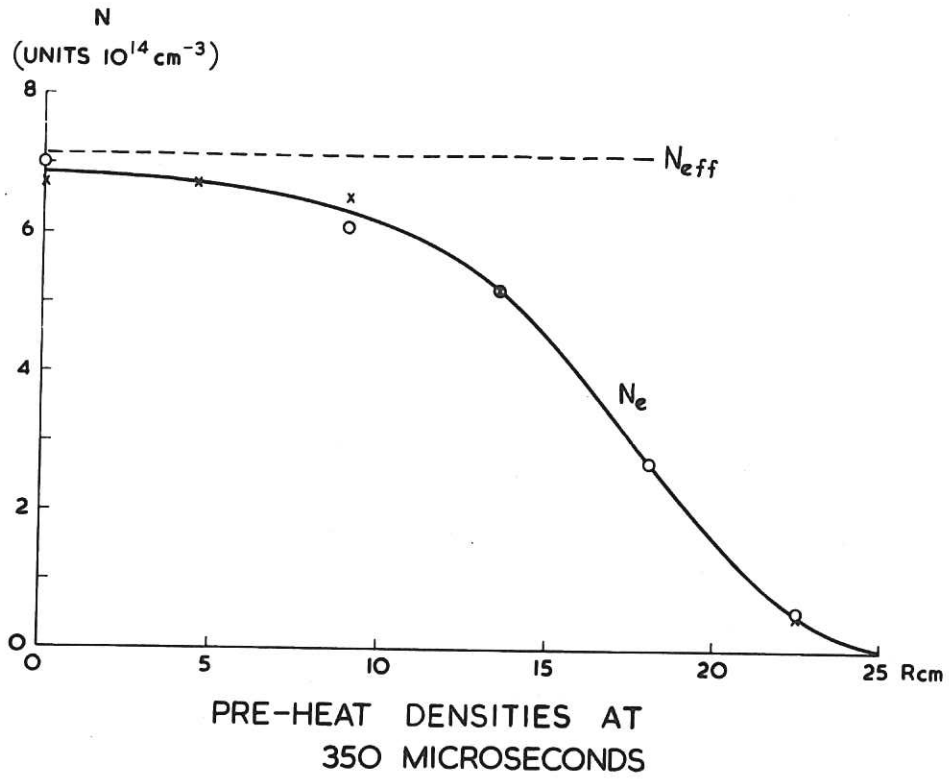

Fig. 1 (CLM-P 92)
Radial variation of electron density (N_e) and total density (N_{eff})

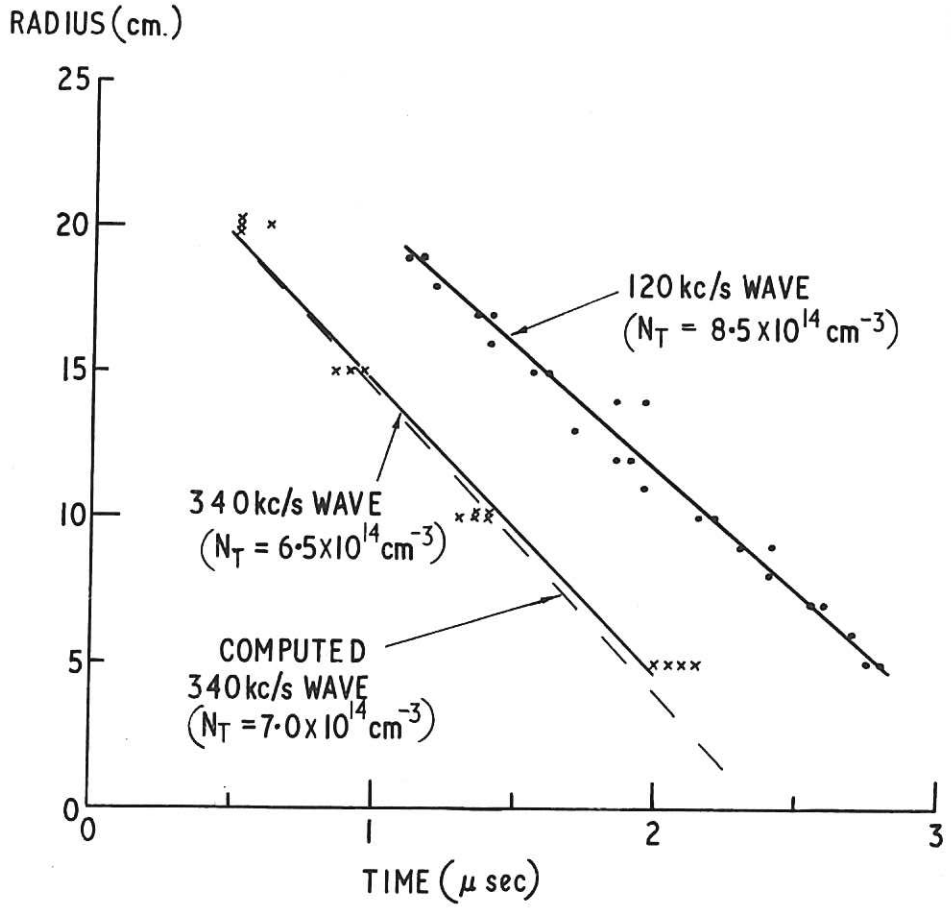

Fig. 2 Space-time streaks of magnetosonic waves (CLM-P 92)

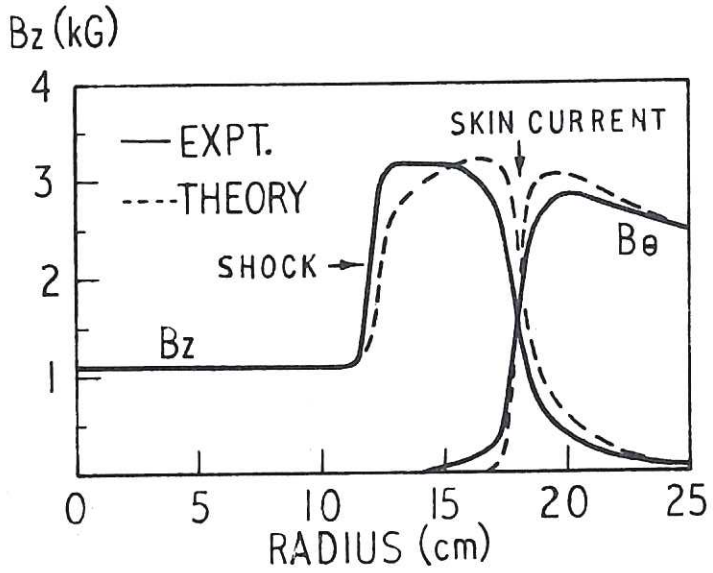

Fig. 3 (CLM-P92)
Radial variation of B_z and B_θ at 0.9 μsec for V_o= 50 kV, P_o = 20 mT H_2, B_{zo} = 1.15 kG

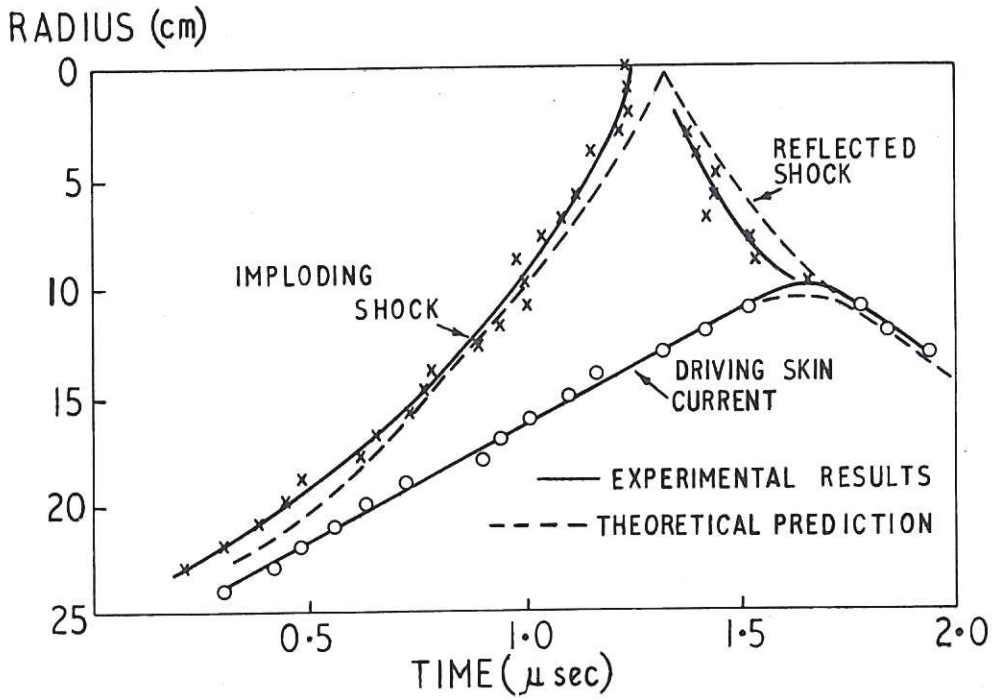

Fig. 4 (CLM-P92)
Space-time streak of implosion for V_o = 50 kV, P_o = 20 mT H_2, B_{zo} = 1.15 kG

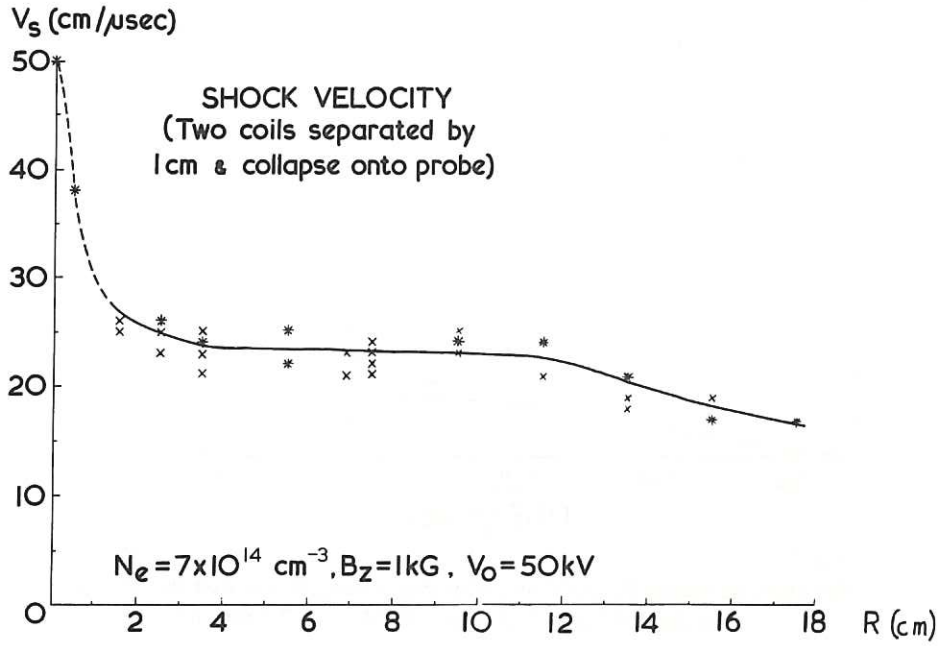

Fig. 5 Radial variation of shock velocity (CLM-P 92)

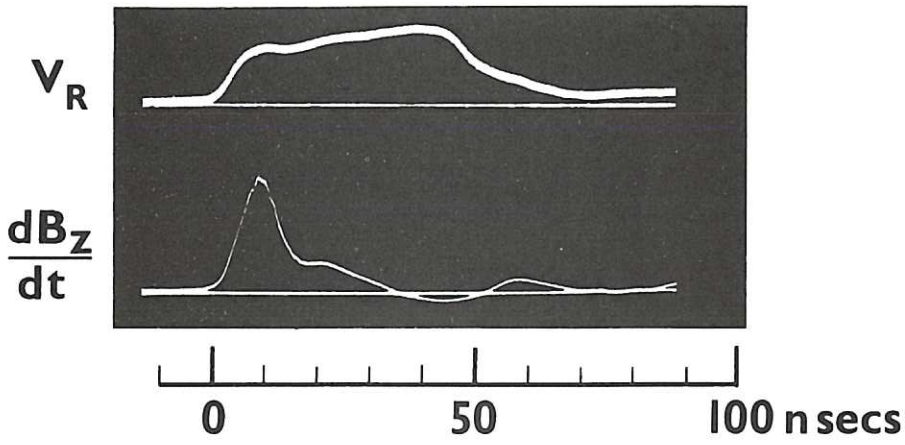

Fig. 6 (CLM-P 92)
Oscillograms of shock structure at 9 cm radius for $M_A = 2.5$ in hydrogen

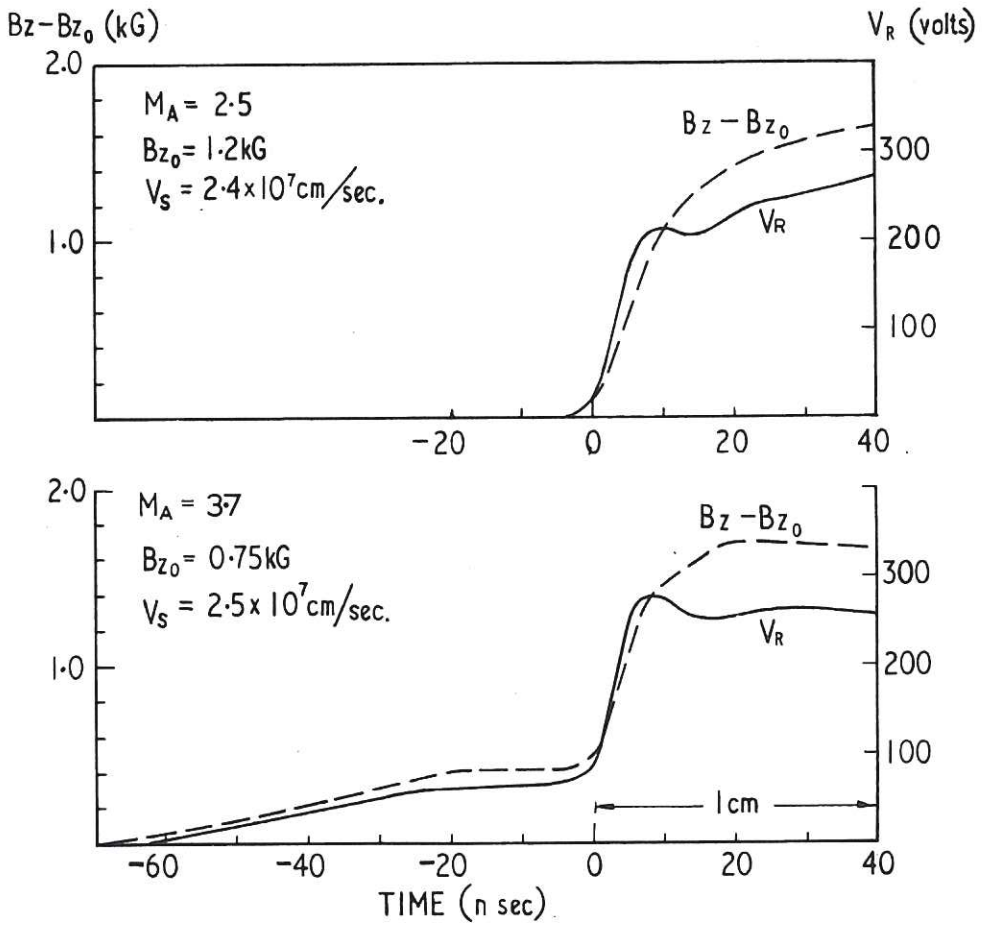

Fig. 7 (CLM-P 92)
Structure of magnetic field and electric potential through the shock front for (a) $M_A = 2.5$ (top) (b) $M_A = 3.7$ (bottom)

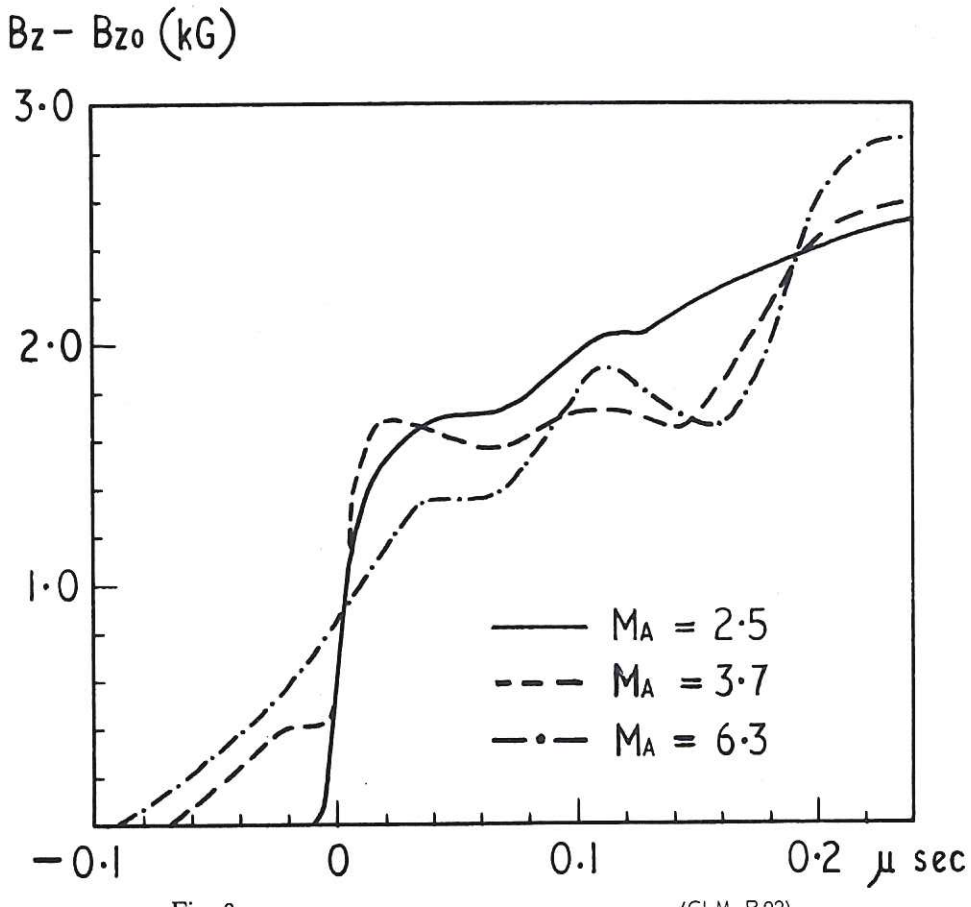

Fig. 8 (CLM-P 92)
Structure of magnetic field through the shock front for $M_A = 2.5$, 3.7 and 6.3

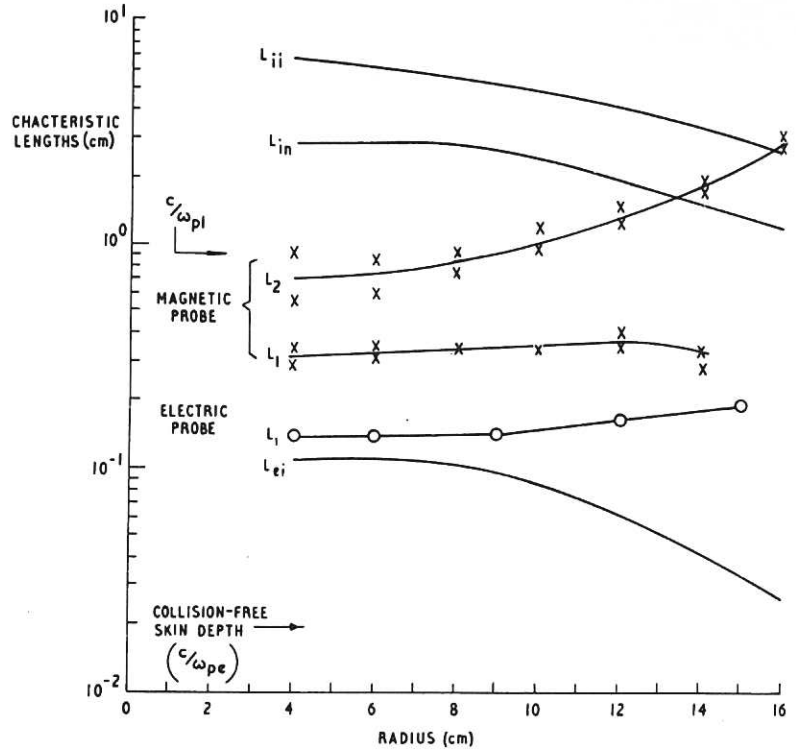

Fig. 9 (CLM-P 92)
Characteristic shock lengths (L_1 is the first fast feature and L_2 the second)

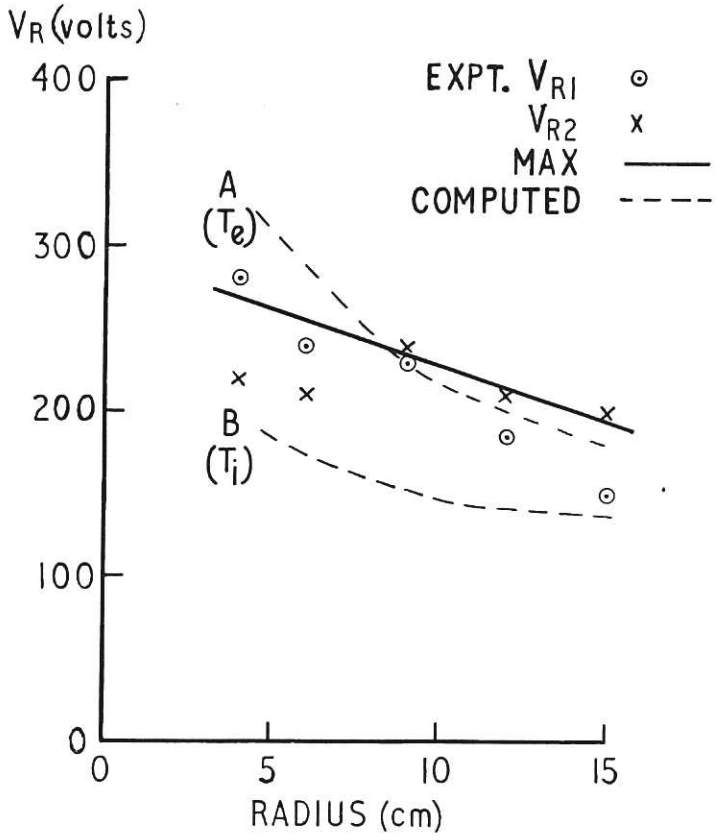

Fig. 10 (CLM-P 92)
Radial variation of radial voltage across the shock front (V_{R1} is from the first fast feature and V_{R2} from the second)